

Thermodynamic Evidence for a Two-Component Superconducting Order Parameter in Sr_2RuO_4

Sayak Ghosh,¹ Arkady Shekhter,² F. Jerzembeck,³ N. Kikugawa,⁴ Dmitry A. Sokolov,³
Manuel Brando,³ A. P. Mackenzie,³ Clifford W. Hicks,³ and B. J. Ramshaw^{*1}

¹*Laboratory of Atomic and Solid State Physics,
Cornell University, Ithaca, NY 14853, USA*

²*National High Magnetic Field Laboratory,
Florida State University, Tallahassee, FL 32310, USA*

³*Max Planck Institute for Chemical Physics of Solids, Dresden, Germany*

⁴*National Institute for Materials Science, Tsukuba, Ibaraki 305-0003, Japan*

Sr_2RuO_4 has stood as the leading candidate for a spin-triplet superconductor for 26 years. Recent NMR experiments have cast doubt on this candidacy, however, and it is difficult to find a theory of superconductivity that is consistent with all experiments. What is needed are symmetry-based experiments that can rule out broad classes of possible superconducting order parameters. Here we use resonant ultrasound spectroscopy to measure the entire symmetry-resolved elastic tensor of Sr_2RuO_4 through the superconducting transition. We observe a thermodynamic discontinuity in the shear elastic modulus c_{66} , requiring that the superconducting order parameter is two-component. A two-component p -wave order parameter, such as $p_x + ip_y$, naturally satisfies this requirement. As this order parameter appears to be precluded by recent NMR experiments, we suggest that two other two-component order parameters, namely $\{d_{xz}, d_{yz}\}$ or $\{d_{x^2-y^2}, g_{xy(x^2-y^2)}\}$, are now the prime candidates for the order parameter of Sr_2RuO_4 .

INTRODUCTION

Nearly all known superconductors are “spin-singlet”, composed of Cooper pairs that pair spin-up electrons with spin-down electrons. Noting that Sr_2RuO_4 has similar normal-state properties to superfluid ^3He , Rice and Sigrist[1] and, separately, Baskaran [2], suggested that Sr_2RuO_4 may be a solid-state “spin-triplet” superconductor. This attracted the attention of the experimental community, and ensured decades of intense research on Sr_2RuO_4 that resulted in a detailed understanding of its metallic state [3, 4]. From this well-understood starting point one might expect the superconductivity of Sr_2RuO_4 to be a solved problem [5], but decades after its discovery the symmetry of the superconducting order parameter remains a mystery, largely due to discrepancies between several major pieces of experimental evidence [6].

Formerly, the strongest evidence for spin-triplet pairing in Sr_2RuO_4 was a Knight shift that was unchanged upon entering the superconducting state [7]. A recently revised version of this experiment, however, shows that the Knight shift is suppressed below T_c , ruling against most spin-triplet order parameters [8, 9]. This is consistent with measurements of the upper-critical magnetic field, which appears to be Pauli-limited and thus suggests spin-

singlet pairing [10]. The challenge is to reconcile these data with previous evidence in favour of a spin-triplet order parameter, including time-reversal symmetry breaking below T_c in μ SR[11] and polar Kerr effect experiments[12], and half-quantized vortices [13].

While the spin-triplet versus spin-singlet aspect of the superconductivity in Sr_2RuO_4 is still under debate, less well studied is the symmetry of the orbital part of the Cooper pair wavefunction. By symmetry, spin-triplet superconductors are required to have an odd-parity orbital wavefunction, i.e. to be an $l = 1$ ‘ p -wave’ or $l = 3$ ‘ f -wave’ superconductor, where l is the orbital quantum number. This is in contrast with conventional $l = 0$ s -wave superconductors, or the high- T_c $l = 2$ d -wave superconductors. While some information about the orbital wavefunction can be inferred by looking for nodes in the superconducting gap, determination of nodal position does not uniquely determine the orbital structure of the Cooper pair.

One way to distinguish different orbital states is by their degeneracy—the number of states with the same energy. s -wave and $d_{x^2-y^2}$ -wave Cooper pairing states, for example, are both singly degenerate (“one-component”), while the $\{p_x, p_y\}$ state (which can order in the chiral $p_x + ip_y$ configuration) is two-fold degenerate (“two-component”). This difference in orbital degeneracy has an unambiguous signature in an ultrasound experiment: shear elastic moduli are continuous through T_c for a singly-degenerate orbital state, but are discontinuous across T_c for a doubly degenerate state [14, 15]. The observation of a discontinuity in one of the shear elastic moduli of Sr_2RuO_4 at T_c would therefore constitute strong evidence in favour of either p -wave superconductivity, or one of the other two-component superconducting order parameters. These measurements have been attempted in the past, and were suggestive of a shear discontinuity at T_c , but a discontinuity was also found in a symmetry-forbidden channel, and the experiment was thus deemed to be inconclusive [16]. Other independent evidence of a shear discontinuity [17] is now being submitted as part of a separate complementary study using an experimental technique different from our own (for a theoretical interpretation of these results, see Walker and Contreras [18]).

EXPERIMENT

Elastic moduli are second derivatives with respect to strain of a system’s total free energy. Elastic moduli are therefore thermodynamic coefficients akin to heat capacity or magnetic

		Compression		Shear	
Coupling to order parameter					
		Representation	A_{1g}	B_{1g}	B_{2g}
		Elastic modulus	$(c_{11}+c_{12})/2$	$(c_{11}-c_{12})/2$	c_{66}
		One-component e.g. “d-wave” $\eta \sim d_{x^2-y^2}$	$\epsilon_{A_{1g}} \cdot \eta^2$ ✓	✗	✗
		Two-component e.g. “p-wave” $\eta \sim (\rho_x, \rho_y)\hat{z}$	$\epsilon_{A_{1g}} \cdot (\eta_x^2 + \eta_y^2)$ ✓	$\epsilon_{B_{1g}} \cdot (\eta_x^2 - \eta_y^2)$ ✓	$\epsilon_{B_{2g}} \cdot (\eta_x \eta_y)$ ✓

FIG. 1. **Irreducible strains in Sr_2RuO_4 and their coupling to superconducting order parameters.** The tetragonal crystal structure of Sr_2RuO_4 and unit cell deformations illustrating the irreducible representations of strain are shown. There is an elastic modulus corresponding to each of these strains, and a sixth modulus c_{13} that arises from coupling between the two A_{1g} strains. Green check marks denote allowed linear-order couplings to strain for one and two-component order parameter bilinears, and red crosses denote that such coupling is forbidden. These couplings are what lead to discontinuities in the elastic moduli at T_c . See Table I for a list of relevant possible order parameters in Sr_2RuO_4 .

susceptibility, and are indicative of a system’s ground-state properties. Strain is a second-rank tensor quantity, and thus it can couple to order parameters in ways that lower-rank quantities, such as temperature and electric field, cannot. This, in particular, requires that elastic moduli behave differently in systems with one- or two-component order parameters. Here we provide a brief overview of the connection between crystal symmetry, order parameter symmetry, and ultrasound: the detailed derivations can be found in the ‘Strain-Order Parameter Coupling’ section in S.I., as well as in a number of theoretical papers [14, 18, 19].

The allowed couplings between strains and superconducting order parameters become transparent when both are described in terms of irreducible representations (irreps) of the

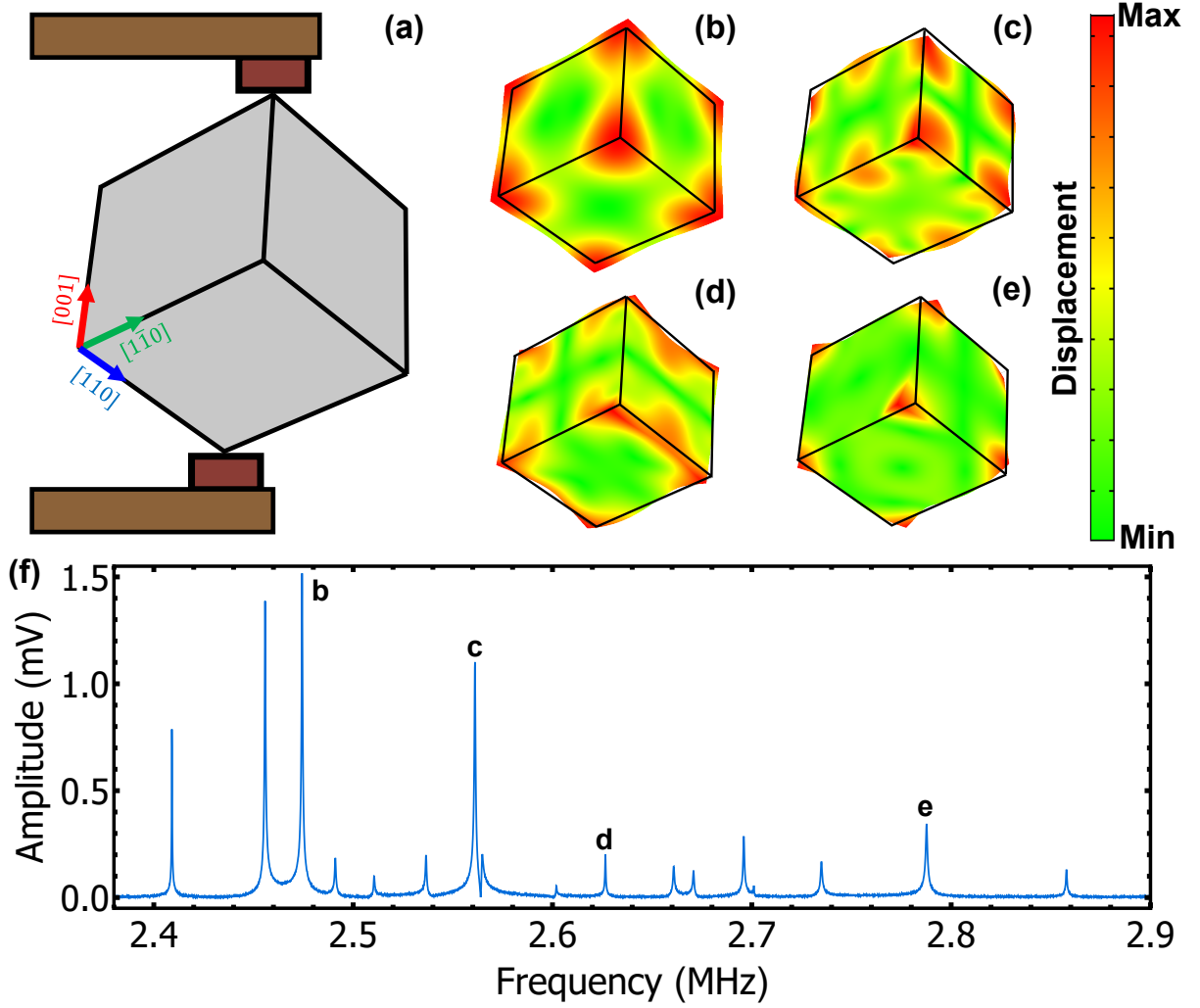


FIG. 2. **Resonant ultrasound spectroscopy: schematic and spectrum.** (a) A single-crystal sample, polished along known crystal axes, is held in weak-coupling contact between two ultrasonic transducers, allowing it to vibrate freely at its resonance frequencies. Panels (b) through (e) show the crystal's deformation corresponding to four particular experimentally measured resonances, marked in (f). (f) A portion of the ultrasonic spectrum of Sr_2RuO_4 , in the frequency range from 2.4-2.9 MHz, taken at room temperature. Each resonance creates a unique strain pattern in the material that can be decomposed in terms of the five irreducible strains (Figure 1(a)), modulated in phase along the dimensions of the sample.

point-group symmetry. Sr_2RuO_4 crystallizes in the tetragonal space group $I4/mmm$, along with its associated point group D_{4h} . In this crystal field environment, the five-component $l = 2$ d -representation breaks into three one-component irreps: d_{z^2} (A_{1g} irrep), d_{xy} (B_{2g}), and

$d_{x^2-y^2}$ (B_{1g} —the familiar ‘ d -wave’ of the cuprates), and one two-component irrep $\{d_{xz}, d_{yz}\}$ (E_g). The three-component p -representation breaks into the one-component irrep p_z (A_{2u}) and the two-component irrep $\{p_x, p_y\}$ (E_u)—it is this latter representation that has been proposed to order into the chiral $p_x + ip_y$ superconducting state.

As illustrated in Figure 1, there are five unique strains (ϵ_Γ) in Sr_2RuO_4 (five irreps (Γ) of strain in D_{4h}): two compressive strains transforming as the A_{1g} irrep, and three shear strains transforming as the B_{1g} , B_{2g} and E_g irrep. Each strain has a corresponding elastic modulus, $c_\Gamma = \partial^2 \mathcal{F} / \partial \epsilon_\Gamma^2$, where \mathcal{F} is the thermodynamic free energy. A sixth modulus, c_{13} , defines the coupling between the two A_{1g} strains ($\epsilon_{xx} + \epsilon_{yy}$ and ϵ_{zz} .) Sound velocities can be computed from these moduli as $v_\Gamma = \sqrt{c_\Gamma / \rho}$, where ρ is the density. When composing terms in the free energy, direct (linear) coupling between strain and the superconducting order parameter (η) is forbidden because superconductivity breaks gauge symmetry. The next relevant coupling is linear in strain and quadratic in order parameter. For one-component superconducting order parameters, including all s -wave states and the $d_{x^2-y^2}$ state, the only quadratic form is η^2 , transforming as A_{1g} , and thus the only allowed coupling is $\epsilon_{A_{1g}} \eta^2$. This coupling produces discontinuities in all the A_{1g} (compressional) elastic moduli across T_c . Two-component order parameters ($\vec{\eta} = \{\eta_x, \eta_y\}$), on the other hand, have three independent quadratic forms: $\eta_x^2 + \eta_y^2$, $\eta_x^2 - \eta_y^2$, and $\eta_x \eta_y$, transforming as A_{1g} , B_{1g} , and B_{2g} , respectively. Thus in addition to coupling to the A_{1g} elastic moduli, two-component order parameters couple to two of the shear moduli through $\epsilon_{B_{1g}} (\eta_x^2 - \eta_y^2)$ and $\epsilon_{B_{2g}} \eta_x \eta_y$. This produces discontinuities in the associated shear elastic moduli ($(c_{11} - c_{12})/2$ and c_{66} , respectively), based purely on symmetry considerations, and independent of the microscopic mechanism of superconductivity.

While traditional pulse-echo ultrasound experiments measure a single elastic modulus per experiment, we use resonant ultrasound spectroscopy (RUS) to measure all six elastic moduli of Sr_2RuO_4 across T_c in a single experiment, greatly reducing systematic uncertainty [20]. Analogous to how a stretched string has standing waves that can be expressed in terms of sinusoidal harmonics, three-dimensional solids have elastic resonances that can be decomposed in terms of the irreps of strain. RUS measures the frequencies of these resonances for a single crystal sample, from which all elastic moduli can be obtained by inverse-solving the elastic wave equation [21]. The relatively low T_c (≈ 1.43 K for our sample) of Sr_2RuO_4 , however, poses severe technical challenges to perform RUS experiments across T_c . RUS samples are typically large (of the order 1 mm³), and are only in weak-coupling

contact with the transducers (see Figure 2(a)). This ensures nearly-free boundary conditions but prevents good thermal coupling between the apparatus and the sample. Previous RUS implementations either sacrificed uniform cooling by placing the sample in vacuum [21], or sacrificed a slow cooling rate by placing the sample in direct thermal contact with the helium bath. Our new RUS design employs a double vacuum can arrangement (see Methods for details) to allow for slow, uniform cooling of a sample down to approximately 1.25 K. We observe a sharp (40 mK wide) superconducting transition (Figure 3(a)), signifying high sample quality and uniform sample cooling.

We performed RUS measurements on a single-crystal sample of Sr_2RuO_4 across T_c . The full data set includes 18 resonances (see Figure 5)—five representative resonances are shown in Figure 3(a). We decompose all 18 resonances into the three compressional moduli ($(c_{11} + c_{12})/2$, c_{33} , and c_{13}) and the three shear moduli ($(c_{11} - c_{12})/2$, c_{44} , and c_{66} .) The temperature evolution of these moduli are shown in Figure 3(b) and (c). Discontinuities across T_c are clearly observed in all three compressional moduli, as required by thermodynamics for all superconductors, as well as in the shear modulus c_{66} . The discontinuity in c_{66} is forbidden by symmetry for one-component order parameters, but is allowed for two-component order parameters—this discontinuity is our central finding.

Having measured all six elastic moduli across T_c , we can perform several consistency checks. First, since there is no bilinear coupling of the order parameter to E_g strain, c_{44} should not have a discontinuity at T_c for any superconducting order parameter. Within our experimental uncertainty, we observe only a change in the slope of c_{44} at T_c , which is expected on general grounds and is not constrained by symmetry [14]. Second, thermodynamics dictates that the discontinuities in the three compressional moduli at a second order phase transition should follow a self-consistency relation (see discussion preceding Equation S16 in S.I.),

$$\left(\Delta \frac{c_{11} + c_{12}}{2}\right) \times (\Delta c_{33}) = (\Delta c_{13})^2. \quad (1)$$

From our measurement, we find $(\Delta \frac{c_{11} + c_{12}}{2}) \times (\Delta c_{33}) = (9.9 \pm 1.5) \times 10^{-5} \text{ GPa}^2$ and $(\Delta c_{13})^2 = (8.3 \pm 1.1) \times 10^{-5} \text{ GPa}^2$. These consistency checks validate our measurement of the magnitude of the jumps, and our ability to correctly decompose the jumps in frequency into jumps in the irreducible elastic moduli.

A further check on the data is provided by an Ehrenfest relation that relates the derivative of T_c with hydrostatic pressure, P , to the discontinuities at T_c in the specific heat, ΔC , and

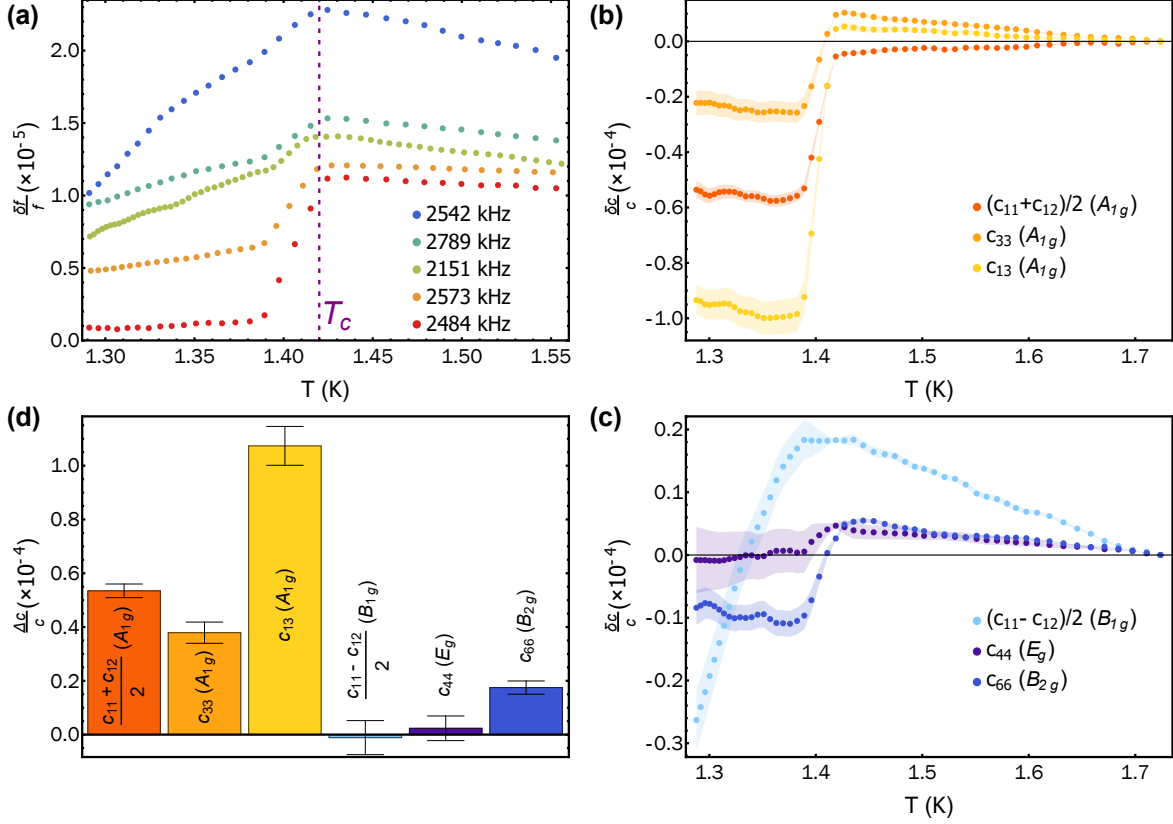


FIG. 3. **Resonant ultrasound spectroscopy across T_c in Sr_2RuO_4 .** (a) Temperature evolution of five representative resonances measured through T_c —plots are shifted vertically for visual clarity. The dashed line shows T_c determined by resistivity measurements. A step-like discontinuity (“jump”) is observed at T_c —the different magnitudes of this jump signify the contributions of different elastic moduli in each resonance. 18 such resonances were tracked through T_c to determine the elastic moduli. (b) Compressional (A_{1g}) and (c) shear (B_{1g} , E_g and B_{2g}) moduli of Sr_2RuO_4 across T_c , along with their experimental errors arising from the uncertainties in sample dimensions. The absolute values of these moduli at 4 kelvin are determined to be $(c_{11} + c_{12})/2 = 190.8$, $c_{33} = 257.2$, $c_{13} = 85.0$, $(c_{11} - c_{12})/2 = 53.1$, $c_{66} = 65.5$ and $c_{44} = 69.5$ GPa. (d) Magnitudes of the elastic moduli jumps at T_c , along with their experimental uncertainties (see ‘Uncertainty Analysis’ in S.I. for details).

the bulk modulus, ΔB , via

$$\left(\frac{dT_c}{dP}\right)^2 = -\frac{\Delta B}{B^2} \left(\frac{\Delta C}{T}\right)^{-1}. \quad (2)$$

We measure $\Delta B/B \approx 6.3 \times 10^{-5}$ (see ‘Ehrenfest Relations for Compressional Strains’ in S.I.).

Combined with $\Delta C/T$ for this sample (see Figure 4), Equation 2 yields a value for dT_c/dP of 0.90 K/GPa. This is a factor of 3 higher than what is reported for a direct measurement of T_c as a function of pressure [22]. This discrepancy may be evidence for a pair of transitions occurring at or near the superconducting T_c , as discovered by recent μ SR experiments [23]. The two transition temperatures split when stress is applied along the x direction—Meissner screening onsets at the higher transition temperature, T_c , while time reversal symmetry is broken at the lower transition, T_{TRSB} . To perform the correct Ehrenfest analysis one would require dT_{TRSB}/dP , which is unknown at present. A similar Ehrenfest relation—derived for the jump in c_{66} rather than the jump in bulk modulus—requires that T_c shift linearly with B_{2g} strain, specifically as $T_c \propto |\epsilon_{xy}|$. Prior measurements of T_c as a function of ϵ_{xy} , however, have not found this linear dependence on strain [24]. In addition, most ordered states of two-component order parameters should exhibit two transition temperatures under finite strain, but this has not been found either by heat capacity or local susceptibility measurements [25, 26], at least for B_{1g} strain. In the S.I. we show that the current experimental resolution on these phenomena is still consistent with the size of the jump that we find in c_{66} (see ‘Reconciling the c_{66} Discontinuity with Experiments Under Finite Strain’).

DISCUSSION

A discontinuity in c_{66} at T_c can *only* result from a two-component superconducting order parameter (see Table I). This is a critical piece of information because evidence for vertical line nodes in the superconducting gap—from ultrasonic attenuation [17], heat capacity [27], thermal conductivity [28], and quasiparticle interference [29]—are most straightforwardly interpreted in terms of a one-component, $d_{x^2-y^2}$, order parameter. With the discovery of a suppression of the Knight shift strongly suggesting that the order parameter cannot be spin-triplet [8], $d_{x^2-y^2}$ would seem a likely contender. The discontinuity in c_{66} , however, rules against *any* one-component order parameter, including $d_{x^2-y^2}$.

Our measurement is consistent with several two-component p -wave scenarios, including $(p_x \pm ip_y)\hat{z}$ and $p_z(\hat{x} \pm i\hat{y})$. Taken at face value, however, the suppression of the Knight shift [8] rules out all p -wave order parameters, and is consistent only with spin-singlet order parameters. The only “conventional” spin-singlet order parameter that produces a jump in c_{66} at T_c is $\{d_{xz}, d_{yz}\}$. This state can order into the non-magnetic d_{xz} , d_{yz} , or $d_{xz} \pm d_{yz}$

Dimensionality	Order Parameter	Irrep.	Moduli Jumps	Ultrasound	NMR
One-component	s	A_{1g}	A_{1g}	\times	\checkmark
	$d_{x^2-y^2}$	B_{1g}	A_{1g}	\times	\checkmark
	d_{xy}	B_{2g}	A_{1g}	\times	\checkmark
Two-component	$\{p_x, p_y\} \hat{\mathbf{z}}$	E_u	A_{1g}, B_{1g}, B_{2g}	\checkmark	\times
	$p_z \{\hat{\mathbf{x}}, \hat{\mathbf{y}}\}$	E_u	A_{1g}, B_{1g}, B_{2g}	\checkmark	\times
	$\{d_{xz}, d_{yz}\}$	E_g	A_{1g}, B_{1g}, B_{2g}	\checkmark	\checkmark
	$\{d_{x^2-y^2}, g_{xy(x^2-y^2)}\}$	$B_{1g} \oplus A_{2g}$	A_{1g}, B_{2g}	\checkmark	\checkmark

TABLE I. **Some superconducting order parameters and their representations in D_{4h} .**

For the odd-parity spin-triplet order parameters, $\hat{\mathbf{x}}$, $\hat{\mathbf{y}}$ and $\hat{\mathbf{z}}$ represent the pair wavefunction in spin space in the \mathbf{d} -vector notation [5]. Two component order parameters $\{\eta_x, \eta_y\}$ can order as η_x , η_y , $\eta_x \pm \eta_y$, or $\eta_x \pm i\eta_y$, depending on microscopic details. It is this latter combination that forms the time-reversal symmetry breaking state (e.g. $(p_x + ip_y)\hat{\mathbf{z}}$, or $d_{xz} + id_{yz}$). The ‘‘Ultrasound’’ column indicates whether an order parameter is consistent with a jump in c_{66} at T_c , the ‘‘NMR’’ column indicates whether it is consistent with the suppression of the Knight shift at T_c . Note that the $B_{1g} \oplus A_{2g}$ state does not belong to a single irrep of D_{4h} , and thus transition temperatures of the d and g components must be ‘‘fine-tuned’’ if they are to coincide.

states, all of which break the C_4 rotational symmetry of the lattice. It can also order into the chiral magnetic $d_{xz} \pm id_{yz}$ state. If one considers the possibility of an accidental degeneracy between two order parameters of different representations, producing accidental two-component order parameters, then $\{d_{xy}, s\}$ and $\{d_{x^2-y^2}, g_{xy(x^2-y^2)}\}$ are also consistent with our experiment ($\{d_{x^2-y^2}, s\}$ [30] produces a jump in $(c_{11} - c_{12})/2$ but not in c_{66}). We set aside $\{d_{xy}, s\}$ because it thought to be incompatible with the electronic structure of Sr_2RuO_4 . If one accepts time-reversal symmetry breaking at T_c as a property of Sr_2RuO_4 , there are then two remaining order parameters that are compatible with our experiment: $d_{xz} \pm id_{yz}$, and $d_{x^2-y^2} \pm ig_{xy(x^2-y^2)}$. The absence of a discontinuity in $(c_{11} - c_{12})/2$ implies that there is no order-parameter-bilinear that transforms as B_{1g} , which would rule out $d_{xz} \pm id_{yz}$. It is possible, however, that while a jump in $(c_{11} - c_{12})/2$ is required thermodynamically, it is either unobservably small because the coupling coefficient is small (for microscopic reasons), or the jump is smeared-out due to high ultrasonic attenuation in the B_{1g} channel

[31]. Thus we consider the implications of both the $d_{xz} \pm id_{yz}$ and the $d_{x^2-y^2} \pm ig_{xy(x^2-y^2)}$ superconducting states in Sr_2RuO_4 .

The first of these, $d_{xz} \pm id_{yz}$, is the chiral-ordered state of $\{d_{xz}, d_{yz}\}$ —a two-component E_g representation [32]. There are two main arguments against such a state. First, $\{d_{xz}, d_{yz}\}$ has a horizontal line node at $k_z = 0$, whereas most experiments suggest that the nodes lie along the $[110]$ and $[\bar{1}10]$ directions [17, 27–29]. There is some evidence, however, for a horizontal line node from angle-dependent heat capacity measurements [33]. Second, Sr_2RuO_4 has very weak interlayer coupling [4], and in the limit of weak interlayer coupling, the pairing strength for this state goes to zero. A recent weak-coupling analysis shows that an E_g state can be stabilized by including momentum-dependent spin orbit coupling [34, 35], and such spin-orbit coupling has been quantified by ARPES in Sr_2RuO_4 [36–38]. This variant of the E_g state has Bogoliubov Fermi surfaces (rather than line nodes) that extend along the k_z direction in a manner that may mimic line-nodes as far as experiment is concerned.

The second possibility, $d_{x^2-y^2} \pm ig_{xy(x^2-y^2)}$, is less natural in that $d_{x^2-y^2}$ is a B_{1g} irrep and $g_{xy(x^2-y^2)}$ is an A_{2g} irrep [39]. Order parameters of different representations have, in general, distinct transition temperatures, and therefore the composite $B_{1g} \oplus A_{2g}$ order parameter requires fine-tuning to produce a single superconducting transition. Fine-tuning aside, this state has two attractive features. First, it produces bilinears only in the A_{1g} and B_{2g} channels ($B_{1g} \otimes A_{2g} = B_{2g}$). This would naturally explain why a jump is seen in c_{66} but not in $(c_{11} - c_{12})/2$. Second, this state has line nodes along the $[110]$ and $[\bar{1}10]$ directions [17, 28, 29]. While the $l = 4$, $g_{xy(x^2-y^2)}$ state may seem exotic, it has been shown (in the weak-coupling regime) to be competitive with $d_{x^2-y^2}$ when nearest-neighbor repulsion is accounted for [40].

Both of these two-component order parameters produce a discontinuity in c_{66} , break time reversal symmetry, are Pauli limited in their upper critical field, exhibit a drop in the Knight shift below T_c , and have ungapped quasiparticles. The accidental degeneracy of $d_{x^2-y^2} \pm ig_{xy(x^2-y^2)}$ means that its T_c should split into two transitions under *any* applied strain, and indeed, the aforementioned μSR measurements have found evidence for such a splitting [23]. This suggests that Sr_2RuO_4 may indeed have two nearly degenerate transitions at ambient pressure. Whether or not such a fine-tuned state is tenable to all experiments remains to be seen, but it is now clear that a two-component superconducting order parameter is an essential feature for understanding the unusual superconducting properties of Sr_2RuO_4 .

METHODS

Sample Preparation

High-quality single crystal Sr_2RuO_4 were grown by the floating-zone method, details of which can be found in [41]. A single crystal was oriented along the $[110]$, $[1\bar{1}0]$ and $[001]$ directions, and polished to dimensions $1.50\text{mm} \times 1.60\text{mm} \times 1.44\text{mm}$, with 1.44mm along the tetragonal c -axis. The $[110]$ orientation of the crystal was accounted for when solving for the elastic moduli.

Sample Characterization

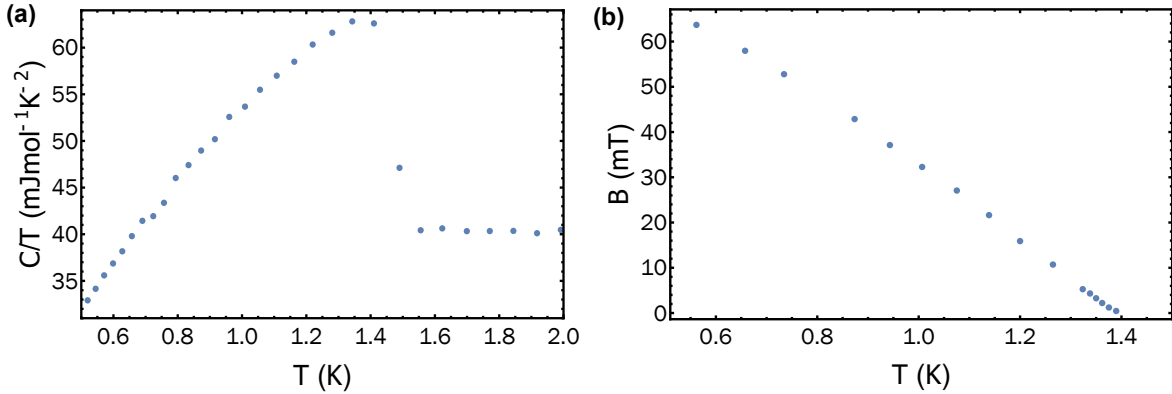


FIG. 4. **Characterization of the Sr_2RuO_4 rod.** (a) Specific heat and (b) susceptibility measurements of the upper critical field, measured on different parts of the same rod from which the sample for RUS experiment was obtained. T_c varies by about 200 mK between different parts of the rod.

The quality of the Sr_2RuO_4 rod from which the RUS sample was cut was characterized by heat capacity and AC susceptibility measurements, shown in Figure 4. Heat capacity measurements of a large piece of the rod exhibit a T_c around 1.45 K, which is close to the optimal T_c [42]. In addition to a relatively high T_c , a low concentration of ruthenium inclusions was an important criterion for the selection of the RUS sample. Ruthenium inclusions locally strain the crystal lattice and can enhance T_c up to 3 K. In order to check for ruthenium inclusions, we measured AC susceptibility by a mutual inductance method,

and found a sharp onset- T_c of 1.43 K, with no sign of a T_c at 3 K, indicating a very low concentration of ruthenium inclusions. The variation in T_c between the heat capacity and the susceptibility/critical field experiments arises because the samples were taken from different parts of the same Sr_2RuO_4 rod. The Sr_2RuO_4 sample for the RUS experiments was also taken from the same rod, and the onset T_c of 1.425 K is in good agreement with the above-mentioned measurements.

Low-Temperature RUS

The relatively low T_c of Sr_2RuO_4 poses several challenges to perform RUS experiments through the superconducting transition. Since RUS samples are typically large (of the order 1 mm^3) and not glued to the transducers (to ensure free boundary conditions), there is weak thermal contact between the sample and its surroundings. Hence, when cooled through T_c , the entire sample may not become superconducting at once, leading to broad superconducting transitions rather than sharp jumps at T_c . To cool below 4.2 K, one could introduce liquid helium into the sample space and pump directly on this space. As RUS is extremely sensitive to vibration, however, this introduces artefacts into the data, and does not provide a particularly homogeneous thermal environment.

To solve these problems the RUS probe was sealed inside a copper can with a small amount of exchange gas, providing good thermal equilibration between the sample, thermometer, and the rest of the apparatus. This inner copper can is separated by a weak thermal link (thin-wall stainless) from an outer brass vacuum can, which provided isolation between the walls of the sample can and the bath. The temperature was regulated by pumping on the external helium bath, and the vacuum isolation of the sample chamber from the bath allows the sample space to then cool very slowly once the bath is pumped to base temperature.

The lowest temperature reached was approximately 1.25 K, as read by a CX-1030 thermometer affixed to the RUS probe. The transition temperature and transition width observed by RUS agree extremely well with those determined from independent susceptibility measurements, suggesting that the Sr_2RuO_4 sample was uniformly thermalized during the experiment.

We measured the temperature dependence of 18 resonances through the superconducting transition—the full data set is shown in Figure 5. The temperature spacing is not identical

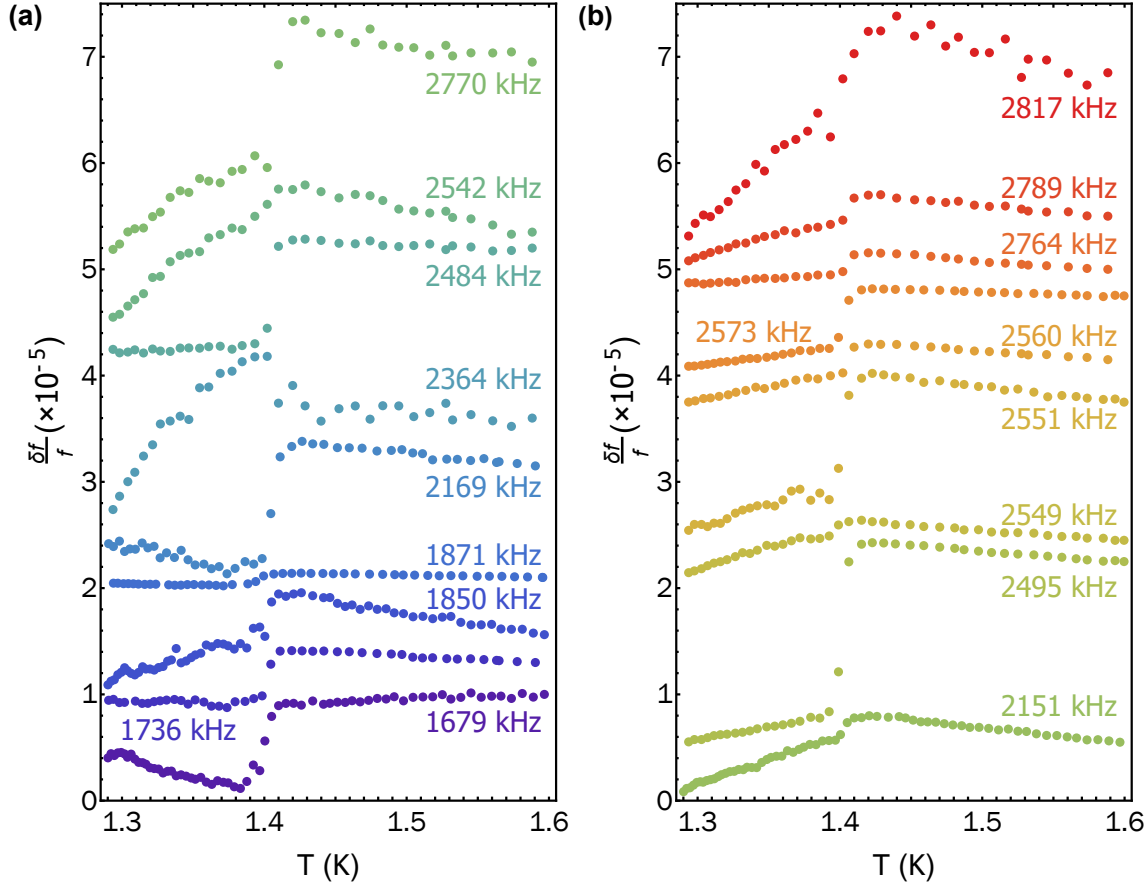


FIG. 5. **RUS frequency data.** Temperature evolution of 18 resonance frequencies of Sr_2RuO_4 through T_c , with panels (a) and (b) each showing 9 frequencies. Plots are vertically shifted for visual clarity.

because the data was acquired over several sweeps through T_c , measuring a few resonances each time. These 18 resonances are then decomposed into the elastic moduli that are shown in Figure 3 of the main text. To do this decomposition we interpolate the frequency versus temperature data, and then plot the elastic moduli at what we consider to be a representative set of temperatures—those from the sweep where we measured the resonances at 2495 kHz, 2549 kHz, and 2551 kHz.

ACKNOWLEDGMENTS

The authors acknowledge helpful discussions with Kimberly Modic, Steve Kivelson, Igor Mazin, Daniel Agterberg, Ronny Thomale, Peter Hirschfeld, Rafael Fernandes, Indranil

Paul, Cyril Proust, and Louis Taillefer.

B.J.R. and S.G. are grateful for help with the experimental design from Eric Smith, Jeevak Parpia, and the LASSP machine shop. B.J.R and S.G. acknowledge support for building the experiment, taking and analyzing the data, and writing the manuscript, from the U.S. Department of Energy, Office of Basic Energy Sciences under Award Number DE-SC0020143. B.J.R. and S.G. acknowledge support by the Cornell Center for Materials Research with funding from the NSF MRSEC program (DMR-1719875). N.K. acknowledges the support from JSPS KAKENHI (No. JP18K04715) in Japan.

AUTHOR CONTRIBUTIONS

S.G. and B.J.R designed the experiment. F.J., D.A.S., N.K., M.B., C.W.H. and A.P.M. prepared the crystal and performed characterization measurements. S.G. acquired and analyzed the ultrasound data. S.G., A.S., C.W.H. and B.J.R. wrote the manuscript with input from all co-authors.

-
- [1] T. M. Rice and M. Sigrist. Sr_2RuO_4 : an electronic analogue of ^3He ? *Journal of Physics: Condensed Matter*, 7(47):L643–L648, nov 1995.
 - [2] G Baskaran. Why is sr_2ruo_4 not a high t_c superconductor? electron correlation, hund’s coupling and p-wave instability. *Physica B: Condensed Matter*, 223:490–495, 1996.
 - [3] Y Maeno, H Hashimoto, K Yoshida, S Nishizaki, T Fujita, JG Bednorz, and F Lichtenberg. Superconductivity in a layered perovskite without copper. *Nature*, 372(6506):532–534, 1994.
 - [4] C. Bergemann, S. R. Julian, A. P. Mackenzie, S. Nishizaki, and Y. Maeno. Detailed topography of the fermi surface of sr_2ruo_4 . *Phys. Rev. Lett.*, 84:2662–2665, Mar 2000.
 - [5] Andrew Peter Mackenzie and Yoshiteru Maeno. The superconductivity of Sr_2RuO_4 and the physics of spin-triplet pairing. *Rev. Mod. Phys.*, 75:657–712, May 2003.
 - [6] Andrew P. Mackenzie, Thomas Scaffidi, Clifford W. Hicks, and Yoshiteru Maeno. Even odder after twenty-three years: the superconducting order parameter puzzle of Sr_2RuO_4 . *npj Quantum Materials*, 2(1):40, 2017.

- [7] K. Ishida, H. Mukuda, Y. Kitaoka, K. Asayama, Z. Q. Mao, Y. Mori, and Y. Maeno. Spin-triplet superconductivity in Sr_2RuO_4 identified by ^{17}O knight shift. *Nature*, 396(6712):658–660, 1998.
- [8] A. Pustogow, Yongkang Luo, A. Chronister, Y.-S. Su, D. A. Sokolov, F. Jerzembeck, A. P. Mackenzie, C. W. Hicks, N. Kikugawa, S. Raghu, E. D. Bauer, and S. E. Brown. Constraints on the superconducting order parameter in Sr_2RuO_4 from oxygen-17 nuclear magnetic resonance. *Nature*, 574(7776):72–75, 2019.
- [9] Kenji Ishida, Masahiro Manago, Katsuki Kinjo, and Yoshiteru Maeno. Reduction of the ^{17}O knight shift in the superconducting state and the heat-up effect by nmr pulses on Sr_2RuO_4 . *Journal of the Physical Society of Japan*, 89(3):034712, 2020.
- [10] S. Kittaka, T. Nakamura, Y. Aono, S. Yonezawa, K. Ishida, and Y. Maeno. Angular dependence of the upper critical field of Sr_2RuO_4 . *Phys. Rev. B*, 80:174514, Nov 2009.
- [11] G. M. Luke, Y. Fudamoto, K. M. Kojima, M. I. Larkin, J. Merrin, B. Nachumi, Y. J. Uemura, Y. Maeno, Z. Q. Mao, Y. Mori, H. Nakamura, and M. Sgrist. Time-reversal symmetry-breaking superconductivity in Sr_2RuO_4 . *Nature*, 394(6693):558–561, 1998.
- [12] Jing Xia, Yoshiteru Maeno, Peter T. Beyersdorf, M. M. Fejer, and Aharon Kapitulnik. High resolution polar kerr effect measurements of Sr_2RuO_4 : Evidence for broken time-reversal symmetry in the superconducting state. *Phys. Rev. Lett.*, 97:167002, Oct 2006.
- [13] J. Jang, D. G. Ferguson, V. Vakaryuk, R. Budakian, S. B. Chung, P. M. Goldbart, and Y. Maeno. Observation of half-height magnetization steps in Sr_2RuO_4 . *Science*, 331(6014):186–188, 2011.
- [14] Walther Rehwald. The study of structural phase transitions by means of ultrasonic experiments. *Advances in Physics*, 22(6):721–755, 1973.
- [15] Sayak Ghosh, Michael Matty, Ryan Baumbach, Eric D. Bauer, K. A. Modic, Arkady Shekhter, J. A. Mydosh, Eun-Ah Kim, and B. J. Ramshaw. One-component order parameter in URu_2Si_2 uncovered by resonant ultrasound spectroscopy and machine learning. *Science Advances*, 6(10), 2020.
- [16] Noriki Okuda, Takashi Suzuki, Zhiqiang Mao, Yoshiteru Maeno, and Toshizo Fujita. Unconventional strain dependence of superconductivity in spin-triplet superconductor Sr_2RuO_4 . *Journal of the Physical Society of Japan*, 71(4):1134–1139, 2002.

- [17] Christian Lupien. *Ultrasound attenuation in the unconventional superconductor Sr_2RuO_4* . PhD Thesis, 2002.
- [18] M. B. Walker and Pedro Contreras. Theory of elastic properties of Sr_2RuO_4 at the superconducting transition temperature. *Phys. Rev. B*, 66:214508, Dec 2002.
- [19] Manfred Sigrist. Ehrenfest Relations for Ultrasound Absorption in Sr_2RuO_4 . *Progress of Theoretical Physics*, 107(5):917–925, 05 2002.
- [20] A. Migliori, J. L. Sarrao, William M. Visscher, T. M. Bell, Ming Lei, Z. Fisk, and R. Gi Leisure. Resonant ultrasound spectroscopic techniques for measurement of the elastic moduli of solids. *Physica B: Condensed Matter*, 183(1-2):1–24, 1993.
- [21] B. J. Ramshaw, Arkady Shekhter, Ross D. McDonald, Jon B. Betts, J. N. Mitchell, P. H. Tobash, C. H. Mielke, E. D. Bauer, and Albert Migliori. Avoided valence transition in a plutonium superconductor. *Proceedings of the National Academy of Sciences*, 112(11):3285–3289, 2015.
- [22] D. Forsythe, S. R. Julian, C. Bergemann, E. Pugh, M. J. Steiner, P. L. Alireza, G. J. McMullan, F. Nakamura, R. K. W. Haselwimmer, I. R. Walker, S. S. Saxena, G. G. Lonzarich, A. P. Mackenzie, Z. Q. Mao, and Y. Maeno. Evolution of fermi-liquid interactions in Sr_2RuO_4 under pressure. *Phys. Rev. Lett.*, 89:166402, Sep 2002.
- [23] Vadim Grinenko, Shreenanda Ghosh, Rajib Sarkar, Jean-Christophe Orain, Artem Nikitin, Matthias Elender, Debarchan Das, Zurab Guguchia, Felix Brückner, Mark E. Barber, Joonbum Park, Naoki Kikugawa, Dmitry A. Sokolov, Jake S. Bobowski, Takuto Miyoshi, Yoshiteru Maeno, Andrew P. Mackenzie, Hubertus Luetkens, Clifford W. Hicks, and Hans-Henning Klauss. Split superconducting and time-reversal symmetry-breaking transitions, and magnetic order in Sr_2RuO_4 under uniaxial stress. *arXiv e-prints*, art. arXiv:2001.08152, January 2020.
- [24] Clifford W. Hicks, Daniel O. Brodsky, Edward A. Yelland, Alexandra S. Gibbs, Jan A. N. Bruin, Mark E. Barber, Stephen D. Edkins, Keigo Nishimura, Shingo Yonezawa, Yoshiteru Maeno, and Andrew P. Mackenzie. Strong increase of T_c of Sr_2RuO_4 under both tensile and compressive strain. *Science*, 344(6181):283–285, 2014.
- [25] Y. S. Li, N. Kikugawa, D. A. Sokolov, F. Jerzembeck, A. S. Gibbs, Y. Maeno, C. W. Hicks, M. Nicklas, and A. P. Mackenzie. High precision heat capacity measurements on Sr_2RuO_4 under uniaxial pressure. *arXiv e-prints*, art. arXiv:1906.07597, Jun 2019.

- [26] Christopher A. Watson, Alexandra S. Gibbs, Andrew P. Mackenzie, Clifford W. Hicks, and Kathryn A. Moler. Micron-scale measurements of low anisotropic strain response of local T_c in Sr_2RuO_4 . *Phys. Rev. B*, 98:094521, Sep 2018.
- [27] Kazuhiko Deguchi, Z. Q. Mao, and Yoshiteru Maeno. Determination of the superconducting gap structure in all bands of the spin-triplet superconductor Sr_2RuO_4 . *Journal of the Physical Society of Japan*, 73(5):1313–1321, 2004.
- [28] E. Hassinger, P. Bourgeois-Hope, H. Taniguchi, S. René de Cotret, G. Grissonnanche, M. S. Anwar, Y. Maeno, N. Doiron-Leyraud, and Louis Taillefer. Vertical line nodes in the superconducting gap structure of Sr_2RuO_4 . *Phys. Rev. X*, 7:011032, Mar 2017.
- [29] Rahul Sharma, Stephen D. Edkins, Zhenyu Wang, Andrey Kostin, Chanchal Sow, Yoshiteru Maeno, Andrew P. Mackenzie, J. C. Séamus Davis, and Vidya Madhavan. Momentum-resolved superconducting energy gaps of Sr_2RuO_4 from quasiparticle interference imaging. *Proceedings of the National Academy of Sciences*, 117(10):5222–5227, 2020.
- [30] A. T. Rømer, D. D. Scherer, I. M. Eremin, P. J. Hirschfeld, and B. M. Andersen. Knight shift and leading superconducting instability from spin fluctuations in Sr_2RuO_4 . *Phys. Rev. Lett.*, 123:247001, Dec 2019.
- [31] C. Lupien, W. A. MacFarlane, Cyril Proust, Louis Taillefer, Z. Q. Mao, and Y. Maeno. Ultrasound attenuation in Sr_2RuO_4 : An angle-resolved study of the superconducting gap function. *Phys. Rev. Lett.*, 86:5986–5989, Jun 2001.
- [32] Igor Žutić and Igor Mazin. Phase-sensitive tests of the pairing state symmetry in Sr_2RuO_4 . *Phys. Rev. Lett.*, 95:217004, Nov 2005.
- [33] Shunichiro Kittaka, Shota Nakamura, Toshiro Sakakibara, Naoki Kikugawa, Taichi Terashima, Shinya Uji, Dmitry A. Sokolov, Andrew P. Mackenzie, Koki Irie, Yasumasa Tsutsumi, Katsuhiko Suzuki, and Kazushige Machida. Searching for gap zeros in Sr_2RuO_4 via field-angle-dependent specific-heat measurement. *Journal of the Physical Society of Japan*, 87(9):093703, 2018.
- [34] Aline Ramires and Manfred Sigrist. Superconducting order parameter of Sr_2RuO_4 : A microscopic perspective. *Phys. Rev. B*, 100:104501, Sep 2019.
- [35] Han Gyeol Suh, Henri Menke, PMR Brydon, Carsten Timm, Aline Ramires, and Daniel F Agterberg. Stabilizing even-parity chiral superconductivity in Sr_2RuO_4 . *arXiv preprint arXiv:1912.09525*, 2019.

- [36] M. W. Haverkort, I. S. Elfimov, L. H. Tjeng, G. A. Sawatzky, and A. Damascelli. Strong spin-orbit coupling effects on the fermi surface of Sr_2RuO_4 and Sr_2RhO_4 . *Phys. Rev. Lett.*, 101: 026406, Jul 2008.
- [37] C. N. Veenstra, Z.-H. Zhu, M. Raichle, B. M. Ludbrook, A. Nicolaou, B. Slomski, G. Landolt, S. Kittaka, Y. Maeno, J. H. Dil, I. S. Elfimov, M. W. Haverkort, and A. Damascelli. Spin-orbital entanglement and the breakdown of singlets and triplets in Sr_2RuO_4 revealed by spin- and angle-resolved photoemission spectroscopy. *Phys. Rev. Lett.*, 112:127002, Mar 2014.
- [38] A. Tamai, M. Zingl, E. Rozbicki, E. Cappelli, S. Riccò, A. de la Torre, S. McKeown Walker, F. Y. Bruno, P. D. C. King, W. Meevasana, M. Shi, M. Radović, N. C. Plumb, A. S. Gibbs, A. P. Mackenzie, C. Berthod, H. U. R. Strand, M. Kim, A. Georges, and F. Baumberger. High-resolution photoemission on Sr_2RuO_4 reveals correlation-enhanced effective spin-orbit coupling and dominantly local self-energies. *Phys. Rev. X*, 9:021048, Jun 2019.
- [39] Steven Allan Kivelson, Andrew Chang Yuan, Brad Ramshaw, and Ronny Thomale. A proposal for reconciling diverse experiments on the superconducting state in Sr_2RuO_4 . *npj Quantum Materials*, 5(1):43, Jun 2020.
- [40] S. Raghu, E. Berg, A. V. Chubukov, and S. A. Kivelson. Effects of longer-range interactions on unconventional superconductivity. *Phys. Rev. B*, 85:024516, Jan 2012.
- [41] Jake S. Bobowski, Naoki Kikugawa, Takuto Miyoshi, Haruki Suwa, Han-shu Xu, Shingo Yonezawa, Dmitry A. Sokolov, Andrew P. Mackenzie, and Yoshiteru Maeno. Improved single-crystal growth of Sr_2RuO_4 . *Condensed Matter*, 4(1), 2019.
- [42] A. P. Mackenzie, R. K. W. Haselwimmer, A. W. Tyler, G. G. Lonzarich, Y. Mori, S. Nishizaki, and Y. Maeno. Extremely strong dependence of superconductivity on disorder in Sr_2RuO_4 . *Phys. Rev. Lett.*, 80:161–164, Jan 1998.
- [43] Wen Huang, Yi Zhou, and Hong Yao. Possible 3D nematic odd-parity pairing in Sr_2RuO_4 : experimental evidences and predictions. *arXiv e-prints*, art. arXiv:1901.07041, Jan 2019.
- [44] Arkady Shekhter, B. J. Ramshaw, Ruixing Liang, W. N. Hardy, D. A. Bonn, Fedor F. Balakirev, Ross D. McDonald, Jon B. Betts, Scott C. Riggs, and Albert Migliori. Bounding the pseudogap with a line of phase transitions in $\text{YBa}_2\text{Cu}_3\text{O}_{6+\delta}$. *Nature*, 498:75 EP –, Jun 2013.
- [45] J. Nyhus, U. Thisted, N. Kikugawa, T. Suzuki, and K. Fossheim. Elastic and specific heat critical properties of $\text{La}_{1.85}\text{Sr}_{0.15}\text{CuO}_4$. *Physica C: Superconductivity*, 369(1):273 – 277, 2002.

- [46] D. Forsythe, S. R. Julian, C. Bergemann, E. Pugh, M. J. Steiner, P. L. Alireza, G. J. McMullan, F. Nakamura, R. K. W. Haselwimmer, I. R. Walker, S. S. Saxena, G. G. Lonzarich, A. P. Mackenzie, Z. Q. Mao, and Y. Maeno. Evolution of fermi-liquid interactions in Sr_2RuO_4 under pressure. *Phys. Rev. Lett.*, 89:166402, Sep 2002.
- [47] K. Fossheim and B. Berre. Ultrasonic propagation, stress effects, and interaction parameters at the displacive transition in SrTiO_3 . *Phys. Rev. B*, 5:3292–3308, Apr 1972.

SUPPLEMENTARY INFORMATION

Thermal Homogeneity Below T_c

While the presence of exchange gas in the sample space ensures that all sample surfaces are at a uniform temperature (which is the same temperature read by the thermometer), we rely on good thermal conduction for the sample interior to equilibrate with the surfaces. Above T_c , normal state Sr_2RuO_4 is a good metal which conducts heat well, and thus the entire volume of the sample should be in thermal equilibrium with surroundings. Below T_c , however, temperature gradients may be enhanced due to the loss of heat carriers, as Cooper pairs do not carry heat. We expect this not to be an issue since Sr_2RuO_4 is a nodal superconductor, which means that there are always normal quasiparticles that carry heat, and the lowest temperature we reach is $\sim 0.8T_c$, which means that the superconducting gap has only partially opened.

To confirm that the thermal gradients in our sample are always small, we perform a simple calculation starting from the 3-dimensional heat flow equation,

$$\frac{\partial T}{\partial t} = \alpha \nabla^2 T, \quad (3)$$

where $T(x, y, z, t)$ denotes the temperature profile within the sample, and α is the thermal diffusivity. For tetragonal Sr_2RuO_4 , this takes the form

$$\frac{\partial T}{\partial t} = \alpha_a \left(\frac{\partial^2 T}{\partial x^2} + \frac{\partial^2 T}{\partial y^2} \right) + \alpha_c \frac{\partial^2 T}{\partial z^2}. \quad (4)$$

The thermal diffusivity α is related to the thermal conductivity κ as $\alpha = \kappa/\rho C$, where ρ is the density of Sr_2RuO_4 and C is the specific heat. For Sr_2RuO_4 below T_c , we have $C = 87 \text{ mJmol}^{-1}\text{K}^{-1}$, $\kappa_a = 13.05 \text{ Wm}^{-1}\text{K}^{-1}$ and $\kappa_c = 0.07 \text{ Wm}^{-1}\text{K}^{-1}$, giving $\alpha_a = 8.61 \times 10^{-3} \text{ m}^2/\text{s}$ and $\alpha_c = 0.05 \times 10^{-3} \text{ m}^2/\text{s}$.

We first consider the effects of a step-change in the exchange-gas temperature as a worst-case scenario. With the boundary condition that all sample surfaces are at T_0 , the solution of Equation 4 is

$$T(x, y, z, t) = T_0 + \sum_{m,n,p=1}^{\infty} A_{mnp} \sin\left(\frac{m\pi x}{L_x}\right) \sin\left(\frac{n\pi y}{L_y}\right) \sin\left(\frac{p\pi z}{L_z}\right) \cdot \exp\left(-\pi^2 \left(\frac{\alpha_a m^2}{L_x^2} + \frac{\alpha_a n^2}{L_y^2} + \frac{\alpha_c p^2}{L_z^2}\right) t\right), \quad (5)$$

where m, n, p are integers, L_x, L_y, L_z are the sample dimensions, and the coefficients A_{mnp} depend on the initial temperature profile $T(x, y, z, t = 0)$ within the sample. Thus, temperature variations from T_0 within the sample die out exponentially fast and, in the $t \rightarrow \infty$ limit, $T(x, y, z) \rightarrow T_0$. In particular, the slowest equilibration occurs when $A_{111} \neq 0$ and all other $A_{mnp} = 0$, since higher harmonic components have a faster exponential decay. In this case, Equation 5 simplifies to

$$T(x, y, z, t) = T_0 + A_{111} \sin\left(\frac{\pi x}{L_x}\right) \sin\left(\frac{\pi y}{L_y}\right) \sin\left(\frac{\pi z}{L_z}\right) \cdot \exp\left(-\pi^2 \left(\frac{\alpha_a}{L_x^2} + \frac{\alpha_a}{L_y^2} + \frac{\alpha_c}{L_z^2}\right) t\right). \quad (6)$$

The temperature in the middle of the sample ($T_{mid}(t) = T(L_x/2, L_y/2, L_z/2, t)$) differs most from T_0 at $t = 0$, hence we can just look at T_{mid} to get an upper bound on how long it takes for the entire sample to come to T_0 .

$$T_{mid}(t) - T_0 = \Delta T \exp\left(-\pi^2 \left(\frac{\alpha_a}{L_x^2} + \frac{\alpha_a}{L_y^2} + \frac{\alpha_c}{L_z^2}\right) t\right) = \Delta T \exp\left(-\frac{t}{14 \mu\text{s}}\right), \quad (7)$$

where we have used the dimensions of the sample ($1.50\text{mm} \times 1.60\text{mm} \times 1.44\text{mm}$), and we have used the worst-case diffusivity taken below T_c from the thermal conductivity data reported in Hassinger et al. [28] and using the specific heat measured on the same rod our sample came from (see Figure 4). Equation 7 shows that if a temperature difference ΔT appears within the sample, it reduces by a factor of 1000 in less than 10^{-4} s. For comparison, we cool the sample at ≈ 0.3 mK/s, and acquire a data point roughly ever 10 mK. Thus the equilibration time is much faster than time scale over which we do our measurements.

Another consideration is the total temperature offset in the center of the sample as we sweep the temperature, which is not captured by Equation 7. The steady-state solution of Equation 4 for a constant cooling rate results in parabolic temperature profile inside the sample. The steady state profile T_{eq} is given by,

$$T_{eq}(x, y, z) = T_0 + 64 \frac{x(L_x - x)y(L_y - y)z(L_z - z)}{L_x^2 L_y^2 L_z^2} \delta T \quad (8)$$

Clearly, $T_{eq} = T_0$ at the sample surfaces, and the middle of sample is at $T_0 + \delta T$. The offset δT can be calculated by evaluating Equation 3 at $(x = L_x/2, y = L_y/2, z = L_z/2)$ and using the cooling rate $(\partial T / \partial t = 0.3 \text{ mK/s})$,

$$\delta T = \frac{\partial T / \partial t}{8 \left(\frac{\alpha_a}{L_x^2} + \frac{\alpha_a}{L_y^2} + \frac{\alpha_c}{L_z^2} \right)} \approx 6 \text{ nK}. \quad (9)$$

Immediately below T_c , the heat capacity increases by approximately 50%. Over our full temperature range, the thermal conductivity κ_a drops by about 10% [28]. The thermal diffusivity therefore drops by $\approx 50\%$ below T_c . Even with this relatively large change in diffusivity, our results above demonstrate that our sample is very homogeneous in temperature during the course of the RUS experiment—both above and below T_c .

Uncertainty Analysis

While visual inspection is usually sufficient to determine whether or not a particular modulus shows a discontinuity at T_c , numerical values are needed to perform consistency checks on the data, and to make quantitative predictions for future experiments.

One source of uncertainty comes from the width of the superconducting transition. To extract the jump magnitudes and their associated uncertainties in a consistent fashion for all the moduli, we use fits above and below T_c to extrapolate the data across the transition (see Figure 6). We take the jump as the difference between the two extrapolated fits at the experimentally-obtained temperature points between 1.38 K and 1.43 K, which is the width of the superconducting transition. This gives a (non-Gaussian) distribution of modulus jumps that correspond to different T_c assignments. We take the uncertainty to be half the difference of the minimum and maximum jumps, and assign the jump itself to the mean.

A second source of uncertainty comes from the sample dimensions, which are used to extract the elastic moduli from the resonance frequencies. Slight deviations from parallelism, rounding of the sample corners, and other small imperfections give an upper-bound on the dimensional uncertainty of ± 20 microns in each direction. This dimensional uncertainty is then incorporated into the elastic moduli calculations (described in Ramshaw et al. [21]), yielding an uncertainty in the moduli. This gives us the error bars shown for compressional and shear moduli in Figure 3(b) and (c) of main text.

Assuming that the two sources of uncertainty (dimensional uncertainty, and the uncertainty in assigning T_c) are independent, we add them in quadrature to obtain the total uncertainty in each jump, tabulated in Table II.

We have neglected uncertainty due to misalignment of the crystal axes with respect to the sample faces because our crystal was aligned to better than 2° for all 3 axes. The effect

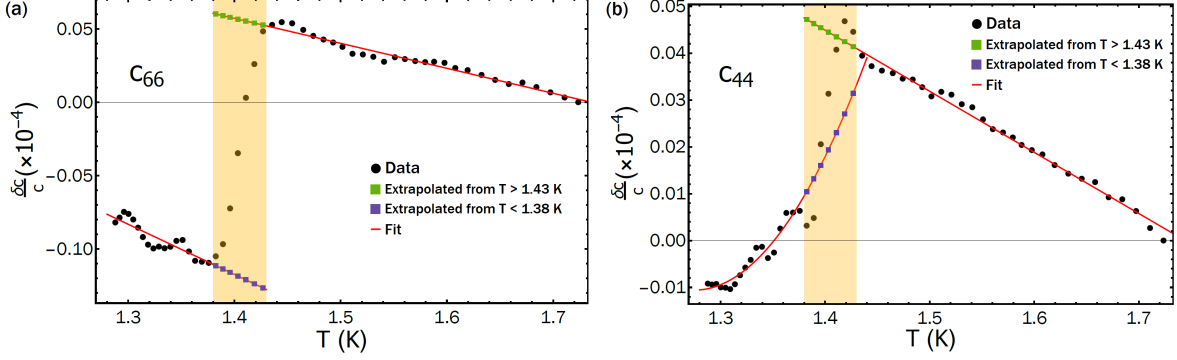


FIG. 6. **Extraction of the jumps in the elastic moduli and their uncertainties.** We extrapolate fits to data (red lines) from above and below T_c at temperature points within the transition (highlighted in yellow). The average between the minimum and maximum jump is taken to be the jump magnitude; the difference is the uncertainty. This procedure is illustrated for c_{66} in panel (a), and c_{44} in panel (b). Note the significantly reduced vertical scale in (b) as compared to (a).

of misalignment can be calculated finding the rotated elastic tensor \mathbf{C}' via

$$C'_{mnop} = R_{mi}R_{nj}R_{ok}R_{pl}C_{ijkl} \quad (10)$$

where \mathbf{C} is the un-rotated elastic tensor and \mathbf{R} is a rotation matrix. For example, a rotation by an angle γ about the a -axis transforms the shear elastic modulus c_{44} as

$$c'_{44} = \frac{1}{4} \left[c_{44} (3 + \cos 4\gamma) + \frac{1}{2} (c_{11} + c_{33} + 2c_{13} (1 - \cos 4\gamma)) \right]. \quad (11)$$

For $\gamma = 2^\circ$, c'_{44} differs from c_{44} by four parts in 10^3 . This introduces a jump into c'_{44} that is 1 part in 10^8 —two orders of magnitude smaller than the other sources of uncertainty. Similar expressions can be derived for the other moduli and are similarly small.

Strain-Order Parameter Coupling

In this section, we calculate expressions for the elastic moduli discontinuities and sound attenuation, starting from a Landau theory. Similar expressions for the chiral state have been calculated by Sigrist [19] and for nematic superconducting states by Huang et al. [43]. Our expressions match those of Sigrist for the chiral state, and we correct the expressions derived by Huang et al. by including all possible order parameter fluctuations. In particular,

Elastic Modulus	$(c_{11} + c_{12})/2$ (A_{1g})	c_{33} (A_{1g})	c_{13} (A_{1g})	$(c_{11} - c_{12})/2$ (B_{1g})	c_{44} (E_g)	c_{66} (B_{2g})
Fractional Jump Size ($\times 10^{-5}$)	5.35	3.79	10.74	-0.07	0.22	1.75
Uncertainty from T_c width ($\times 10^{-5}$)	0.09	0.02	0.10	0.49	0.13	0.04
Uncertainty from Dimensions ($\times 10^{-5}$)	0.24	0.39	0.72	0.41	0.44	0.24
Total Uncertainty ($\times 10^{-5}$)	0.25	0.39	0.72	0.64	0.46	0.25

TABLE II. Summary of jump magnitudes and experimental uncertainties in all six elastic moduli of Sr_2RuO_4 . The two sources of uncertainty—from width of superconducting transition and from sample dimensions—are added in quadrature to get the total uncertainty for each modulus. This leads to our error bars in Figure 3(d) of main text.

we find that both in-plane shear moduli ($(c_{11} - c_{12})/2$ and c_{66}) should show a discontinuity for the nematic states, contrary to what was concluded in [43]. We also show that the three A_{1g} jumps always follow a consistency relation, similar to what was concluded for non-superconducting order parameters in URu_2Si_2 [15], which is also a tetragonal material with point group D_{4h} .

For a two-component superconducting order parameter $\boldsymbol{\eta} = (\eta_x, \eta_y)$, the Landau free energy expansion reads

$$\mathcal{F}_{op}(\boldsymbol{\eta}) = a|\boldsymbol{\eta}|^2 + b_1|\boldsymbol{\eta}|^4 + \frac{b_2}{2} \left((\eta_x^* \eta_y)^2 + (\eta_x \eta_y^*)^2 \right) + b_3 |\eta_x|^2 |\eta_y|^2 + \dots \quad (12)$$

where $a = a_0(T - T_c)$, with $a_0 > 0$, and b_i are phenomenological constants. In a tetragonal crystal, the elastic free energy density is given by

$$\begin{aligned} \mathcal{F}_{el} &= \frac{1}{2} \left(c_{11}(\epsilon_{xx}^2 + \epsilon_{yy}^2) + 2c_{12}\epsilon_{xx}\epsilon_{yy} + c_{33}\epsilon_{zz}^2 + 2c_{13}(\epsilon_{xx} + \epsilon_{yy})\epsilon_{zz} + 4c_{44}(\epsilon_{xz}^2 + \epsilon_{yz}^2) + 4c_{66}\epsilon_{xy}^2 \right) \\ &= \frac{1}{2} \left(\frac{c_{11} + c_{12}}{2}(\epsilon_{xx} + \epsilon_{yy})^2 + c_{33}\epsilon_{zz}^2 + 2c_{13}(\epsilon_{xx} + \epsilon_{yy})\epsilon_{zz} + \frac{c_{11} - c_{12}}{2}(\epsilon_{xx} - \epsilon_{yy})^2 + \right. \\ &\quad \left. 4c_{44}(\epsilon_{xz}^2 + \epsilon_{yz}^2) + 4c_{66}\epsilon_{xy}^2 \right) \\ &= \frac{1}{2} \left(c_{A_{1g,1}}\epsilon_{A_{1g,1}}^2 + c_{A_{1g,2}}\epsilon_{A_{1g,2}}^2 + 2c_{A_{1g,3}}\epsilon_{A_{1g,1}}\epsilon_{A_{1g,2}} + c_{B_{1g}}\epsilon_{B_{1g}}^2 + c_{E_g}|\epsilon_{E_g}|^2 + c_{B_{2g}}\epsilon_{B_{2g}}^2 \right) \end{aligned} \quad (13)$$

where the strains are written as the irreducible representations of D_{4h} , $(\epsilon_{xx} + \epsilon_{yy}) \rightarrow \epsilon_{A_{1g,1}}$, $\epsilon_{zz} \rightarrow \epsilon_{A_{1g,2}}$, $(\epsilon_{xx} - \epsilon_{yy}) \rightarrow \epsilon_{B_{1g}}$, $2\epsilon_{xy} \rightarrow \epsilon_{B_{2g}}$ and $(2\epsilon_{xz}, 2\epsilon_{yz}) \rightarrow \epsilon_{E_g}$.

The lowest order terms that couple strain to the superconducting order parameter must be quadratic in order parameter to preserve gauge symmetry. This coupling gives rise to

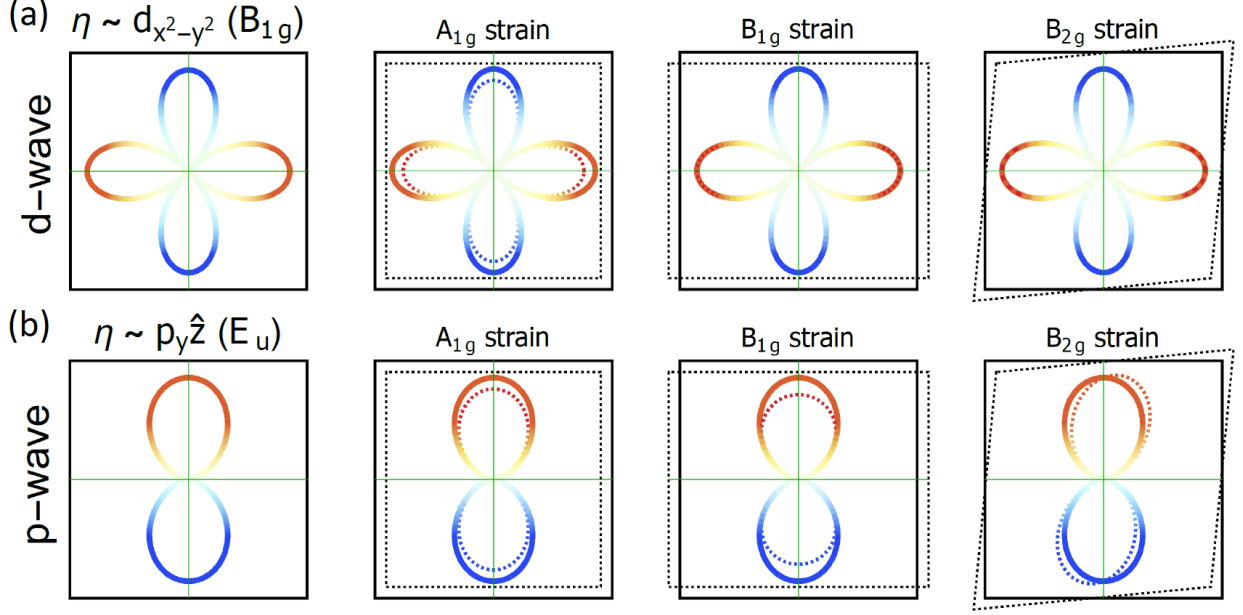


FIG. 7. **Coupling between strain and one/two component order parameters.** (a) Structure of $d_{x^2-y^2}$ gap and (b) $p_y \hat{z}$ gap in k-space, and their couplings to strain. \hat{z} represents the pair wavefunction in spin space. Allowed couplings modify the gap structure in k-space. Only A_{1g} strain couples to one-component order parameters, while A_{1g} , B_{1g} and B_{2g} strain all couple to two-component order parameters.

additional contributions to the free energy

$$\mathcal{F}_c = (g_1 \epsilon_{A_{1g},1} + g_2 \epsilon_{A_{1g},2}) |\boldsymbol{\eta}|^2 + g_4 \epsilon_{B_{1g}} (|\eta_x|^2 - |\eta_y|^2) + g_5 \epsilon_{B_{2g}} (\eta_x^* \eta_y + \eta_x \eta_y^*), \quad (14)$$

where g_i are coupling constants. Coupling between OP and B_{1g} , B_{2g} strains are only allowed for two-component OPs; one-component OPs can only couple to compressive strains (shown for example gap structures in Figure 7). These linear-in-strain, quadratic-in-order-parameter coupling lead to elastic moduli jumps at T_c . Hence jumps in shear moduli can only occur if the OP is two-component. Since no OP can couple to E_g strain, c_{44} should not show a jump at T_c for any superconducting order parameter.

Following Sigrist[19], we use the parameterization $\boldsymbol{\eta} = (\eta_x, \eta_y) = \eta(\cos \theta, e^{i\gamma} \sin \theta)$. Depending on the relative magnitudes of b_1, b_2, b_3 , the system can have different equilibrium OPs[43], characterized by different equilibrium values of $(\theta, \gamma) = (\theta_0, \gamma_0)$: $(\pi/4, \pm\pi/2)$ for the chiral state, $(\pi/4, 0)$ for the diagonal nematic state and $(0, 0)$ for the horizontal nematic state. These states also have different equilibrium values of $\eta = \eta_0$, which can be calculated

from $\partial\mathcal{F}_{op}/\partial\eta|_{(\theta,\gamma)\rightarrow(\theta_0,\gamma_0)} = 0$. Fluctuations of the order parameter amplitude η , orientation θ or relative phase γ can couple to different strains, leading to the jump in corresponding moduli.

To explicitly calculate the moduli discontinuities, we adapt the approach described in [44] to a multi-component OP. For one-component OPs, the discontinuity is

$$c_{mn}^< = c_{mn}^> - \frac{Z_m Z_n}{Y} \implies \Delta c_{mn} = c_{mn}^> - c_{mn}^< = \frac{Z_m Z_n}{Y} \quad (15)$$

where $c_{mn}^< (c_{mn}^>)$ is the elastic modulus below(above) T_c . The thermodynamic coefficients Z_i , Y are defined as $Z_i = \partial^2\mathcal{F}_c/\partial\eta\partial\epsilon_i$ and $Y = \partial^2\mathcal{F}_{op}/\partial\eta^2$. For a multi-component OP $\boldsymbol{\eta}$, Equation 15 gets modified to

$$\Delta c_{mn} = \mathbf{Z}_m^T \mathbf{Y}^{-1} \mathbf{Z}_n \quad (16)$$

where $\mathbf{Z}_i = \partial^2\mathcal{F}_c/\partial\boldsymbol{\eta}\partial\epsilon_i$ and $\mathbf{Y} = \partial^2\mathcal{F}_{op}/\partial\boldsymbol{\eta}^2$ are now matrices. Within this formalism, one can find which OP fluctuation mode couples to a particular strain by looking at the Z_i for that strain. For example, for the chiral state,

$$Z_{A_{1g},1(2)} = \begin{pmatrix} g_{1(2)} \sqrt{\frac{-8a}{4b_1-b_2+b_3}} \\ 0 \\ 0 \end{pmatrix}; Z_{B_{1g}} = \begin{pmatrix} 0 \\ g_4 \frac{4a}{4b_1-b_2+b_3} \\ 0 \end{pmatrix}; Z_{B_{2g}} = \begin{pmatrix} 0 \\ 0 \\ g_5 \frac{2a}{4b_1-b_2+b_3} \end{pmatrix} \quad (17)$$

This shows that η fluctuations couple to the A_{1g} strains, θ fluctuations couple to B_{1g} strain and γ fluctuations couple to B_{2g} strain, consistent with the conclusions of Sigrist [19].

The elastic moduli discontinuities for the various OPs is summarized in Table III. In all cases, the three A_{1g} jumps are found to satisfy the relation

$$\Delta c_{A_{1g},1} \times \Delta c_{A_{1g},2} = (\Delta c_{A_{1g},3})^2 \quad (18)$$

Using the measured jumps in $(c_{11} + c_{12})/2$, c_{33} , and c_{13} (see Figure 3 of the main text and Equation 13), we obtain $(\Delta \frac{c_{11}+c_{12}}{2}) \times (\Delta c_{33}) = (9.9 \pm 1.5) \times 10^{-5} \text{ GPa}^2$, which is in agreement with $(\Delta c_{13})^2 = (8.3 \pm 1.1) \times 10^{-5} \text{ GPa}^2$.

We now turn to order parameter dynamics near the phase transition, which can cause smearing of the frequency jumps. We start with the idea outlined in [44], and adapt it to a multi-component OP. Below T_c , the order parameter relaxation can be modeled as

$$\frac{\partial \tilde{\boldsymbol{\eta}}}{\partial t} = -\boldsymbol{\xi} \frac{\partial \mathcal{F}}{\partial \tilde{\boldsymbol{\eta}}} = -\boldsymbol{\xi} \left(\frac{\partial^2 \mathcal{F}}{\partial \boldsymbol{\eta}^2} \tilde{\boldsymbol{\eta}} + \sum_m \frac{\partial^2 \mathcal{F}}{\partial \boldsymbol{\eta} \partial \epsilon_m} \epsilon_m \right) = -\boldsymbol{\xi} \left(\mathbf{Y} \tilde{\boldsymbol{\eta}} + \sum_m \mathbf{Z}_m \epsilon_m \right) \quad (19)$$

OP	Chiral	Diagonal Nematic	Horizontal Nematic
(θ_0, γ_0)	$(\pi/4, \pm\pi/2)$	$(\pi/4, 0)$	$(0, 0)$
η_0	$\sqrt{\frac{-2a}{4b_1-b_2+b_3}}$	$\sqrt{\frac{-2a}{4b_1+b_2+b_3}}$	$\sqrt{\frac{-a}{2b_1}}$
$\Delta c_{A_{1g},1}$	$\frac{2g_1^2}{4b_1-b_2+b_3} (\eta)$	$\frac{2g_1^2}{4b_1+b_2+b_3} (\eta)$	$\frac{g_1^2}{2b_1} (\eta)$
$\Delta c_{A_{1g},2}$	$\frac{2g_2^2}{4b_1-b_2+b_3} (\eta)$	$\frac{2g_2^2}{4b_1+b_2+b_3} (\eta)$	$\frac{g_2^2}{2b_1} (\eta)$
$\Delta c_{A_{1g},3}$	$\frac{2g_1g_2}{4b_1-b_2+b_3} (\eta)$	$\frac{2g_1g_2}{4b_1+b_2+b_3} (\eta)$	$\frac{g_1g_2}{2b_1} (\eta)$
$\Delta c_{B_{1g}}$	$\frac{2g_4^2}{b_2-b_3} (\theta)$	$\frac{-2g_4^2}{b_2+b_3} (\theta)$	$\frac{g_4^2}{2b_1} (\eta)$
$\Delta c_{B_{2g}}$	$\frac{g_5^2}{b_2} (\gamma)$	$\frac{2g_5^2}{4b_1+b_2+b_3} (\eta)$	$\frac{2g_5^2}{b_2+b_3} (\theta)$

TABLE III. Different equilibrium order parameters and the discontinuities they produce in various elastic moduli. In parentheses, we note fluctuation of which OP mode couples to ultrasound. Jump in compressional (A_{1g}) moduli is always caused by amplitude (η) fluctuations of the OP, whereas for shear modes, jumps can arise from coupling to amplitude (η), orientation (θ) or relative phase (γ) fluctuations.

where $\tilde{\boldsymbol{\eta}}$ are the fluctuations of OP components about equilibrium, and $-\boldsymbol{\xi} \frac{\partial \mathcal{F}}{\partial \tilde{\boldsymbol{\eta}}}$ provides the restoring force towards equilibrium. Assuming linear response of OP fluctuations to strain, when strain is modulated at frequency ω , as in a RUS experiment, Equation 19 becomes

$$-i\omega \tilde{\boldsymbol{\eta}}(\omega) = -\boldsymbol{\tau}^{-1} \tilde{\boldsymbol{\eta}}(\omega) - \boldsymbol{\xi} \sum_m \mathbf{Z}_m \epsilon_m \implies \tilde{\boldsymbol{\eta}}(\omega) = (i\omega \boldsymbol{\tau} - \mathbb{1})^{-1} \mathbf{Y}^{-1} \sum_m \mathbf{Z}_m \epsilon_m \quad (20)$$

where we have defined $\boldsymbol{\tau}^{-1} = \boldsymbol{\xi} \mathbf{Y}$ is the matrix of relaxation times for independent OP modes. For the parameterization $\boldsymbol{\eta} = \eta(\cos \theta, e^{i\gamma} \sin \theta)$,

$$\boldsymbol{\tau} = \begin{pmatrix} \tau_\eta & 0 & 0 \\ 0 & \tau_\theta & 0 \\ 0 & 0 & \tau_\gamma \end{pmatrix} \implies (i\omega \boldsymbol{\tau} - \mathbb{1})^{-1} = \begin{pmatrix} (i\omega \tau_\eta - 1)^{-1} & 0 & 0 \\ 0 & (i\omega \tau_\theta - 1)^{-1} & 0 \\ 0 & 0 & (i\omega \tau_\gamma - 1)^{-1} \end{pmatrix} \quad (21)$$

Using Equation 20, we calculate the dynamic elastic constant as,

$$c_{mn}(\omega) = c_{mn}^> + \frac{\partial^2 \mathcal{F}}{\partial \boldsymbol{\eta} \partial \epsilon_m} \frac{\partial \tilde{\boldsymbol{\eta}}}{\partial \epsilon_n} \implies c_{mn}^<(\omega) = c_{mn}^> + \mathbf{Z}_m^T (i\omega \boldsymbol{\tau} - \mathbb{1})^{-1} \mathbf{Y}^{-1} \mathbf{Z}_n \quad (22)$$

Elastic moduli jumps come from the real part of Equation 22. Depending on which OP mode a particular elastic moduli couples to, the modulus dispersion $c_{mn}(\omega)$ picks up a contribution from the corresponding relaxation time. For example, for the chiral OP,

$$\Delta c_{A_{1g},1(2)} = \frac{2g_{1(2)}^2}{4b_1 - b_2 + b_3} \frac{1}{1 + \omega^2 \tau_\eta^2}; \Delta c_{B_{1g}} = \frac{2g_4^2}{b_2 - b_3} \frac{1}{1 + \omega^2 \tau_\theta^2}; \Delta c_{B_{2g}} = \frac{g_5^2}{b_2} \frac{1}{1 + \omega^2 \tau_\gamma^2}$$

Thus OP relaxation effects can broaden out the elastic moduli jumps, if particular relaxation times are long compared to the experimental frequencies. This has been observed experimentally, for example, in the cuprate superconductor LSCO[45]—higher frequencies reduce the magnitude of jump measured. Since we measure non-zero discontinuities in all the A_{1g} moduli, and the B_{2g} modulus, but no jump in B_{1g} modulus, it is plausible that the B_{1g} jump gets strongly smeared due to this effect. Specifically, for the diagonal nematic state, only the B_{1g} jump is affected by τ_θ , while the other 4 jumps are related to τ_η . Hence if τ_θ is much larger than τ_η for this state, it provides an explanation for the lack of B_{1g} jump. We also note that for this state, close to T_c ($1 - T/T_c \ll 1$), $\tau_\eta^{-1} \propto |a| \propto \eta_0^2 \propto (T_c - T)$ and $\tau_\theta^{-1} \propto \eta_0^4 \propto (T_c - T)^2$. This would indeed make τ_θ much longer than τ_η just below T_c . We also note that large ultrasonic attenuation is observed experimentally in the B_{1g} channel [17], which perhaps motivates the presence of such a long relaxation time.

Reconciling Resonant Ultrasound and Pulse Echo Ultrasound Experiments

The c_{66} discontinuity we measure with RUS is about a factor of 50 larger than what was measured with pulse-echo experiments[17]. This apparent discrepancy may be resolved by looking at the frequency scales of the two experiments: ~ 2.5 MHz for RUS versus 169 MHz for pulse-echo. As noted in the previous section, higher frequencies are expected to reduce the magnitude of the experimentally measured jump. This has been observed at the superconducting transition in $\text{La}_{1.85}\text{Sr}_{0.15}\text{CuO}_4$, where the jump in c_{33} decreases by a factor of ~ 4 when the measurement frequency is increased from 16 MHz to 214 MHz.

Applying a simple relaxation model, like the one derived in the previous section for order-parameter relaxation near the phase transition (Equation 22), we obtain

$$\frac{\Delta c(2.5 \text{ MHz})}{\Delta c(169 \text{ MHz})} = \frac{(1 + (2.5 \text{ MHz} \cdot \tau)^2)^{-1}}{(1 + (169 \text{ MHz} \cdot \tau)^2)^{-1}} = 50 \implies \tau \sim 6.6 \text{ ns} \quad (23)$$

where τ is a relaxation timescale. Applying the same model to the $\text{La}_{1.85}\text{Sr}_{0.15}\text{CuO}_4$ data from Nyhus et al. [45] we obtain 1 ns — a comparable timescale. Whatever the microscopic mechanism underlying this timescale, it is clear that lower-frequency measurements should measure a jump that is closer to the intrinsic thermodynamic jump.

Ehrenfest Relations for Compressional Strains

At the superconducting transition, a jump discontinuity is also measured in the specific heat. Within our formalism, the specific heat jump at T_c , $\Delta C/T$, is calculated as

$$\frac{\Delta C}{T} = \mathbf{W}^T \mathbf{Y}^{-1} \mathbf{W} \quad (24)$$

where $\mathbf{W} = \partial^2 \mathcal{F}_{op} / \partial \boldsymbol{\eta} \partial T$ and $\mathbf{Y} = \partial^2 \mathcal{F}_{op} / \partial \boldsymbol{\eta}^2$. For all three superconducting states discussed above, the A_{1g} moduli jumps can be related to the specific heat jump through

$$\Delta c_{A_{1g},1(2)} = -\frac{\Delta C}{T} \left(\frac{dT_c}{d\epsilon_{A_{1g},1(2)}} \right)^2; \Delta c_{A_{1g},3} = -\frac{\Delta C}{T} \left| \frac{dT_c}{d\epsilon_{A_{1g},1}} \right| \left| \frac{dT_c}{d\epsilon_{A_{1g},2}} \right| \quad (25)$$

It is important to note that such relations for the shear strains are more complicated, and we derive them in the next section. For a tetragonal material, the bulk modulus B is related to the three A_{1g} moduli as

$$B = \frac{\left(\frac{c_{11}+c_{12}}{2} \right) c_{33} - c_{13}^2}{\left(\frac{c_{11}+c_{12}}{2} \right) + c_{33} - 2c_{13}} \quad (26)$$

From Equation 25, the discontinuity in the bulk modulus $\Delta B/B$ at T_c can be related to $\Delta C/T$ through the Ehrenfest relation

$$\frac{\Delta B}{B^2} = -\frac{\Delta C}{T} \left(\frac{dT_c}{dP_{hyd}} \right)^2 \quad (27)$$

where dT_c/dP_{hyd} is the hydrostatic pressure dependence of T_c . Our measurements give $\Delta B/B \sim 6.3 \times 10^{-5}$, about 9 times larger than estimated from specific heat jump and dT_c/dP_{hyd} [46] or, alternatively, the measured jump in the bulk modulus predicts dT_c/dP_{hyd} to be a factor of 3 higher than the measured value. This discrepancy can arise due to the formation of order parameter domains [47], which lead to an additional slowing down of ultrasound and therefore a larger drop in the elastic moduli through T_c . Since these domains would be related to each other by time-reversal in a superconductor, however, it is unclear whether such a mechanism would couple strongly to ultrasound. Another possible cause could be the value of dT_c/dP_{hyd} estimated from the data in [46]. Since the T_c of Sr_2RuO_4 shows a strong increase with B_{1g} strain [24], the measured decrease in T_c under P_{hyd} will be less if the pressure applying medium is not completely hydrostatic. This is particularly relevant because the B_{1g} modulus is almost 4 times smaller than $(c_{11} + c_{12})/2$, which makes it easy to induce B_{1g} strain if the pressure medium is not hydrostatic.

Finally, with the possible discovery of two transitions occurring either simultaneously or near-simultaneously at T_c , it will be necessary to map out T_{TRSB} with pressure to correctly calculate the Ehrenfest relations, which are modified under the presence of two accidentally degenerate order parameters [39].

Ehrenfest Relations for Shear Strains

Unlike A_{1g} strains, shear strains (B_{1g} and B_{2g}) are expected to split the superconducting transition if the OP is a symmetry-protected multi-component order parameter [24]. This happens because shear strains break the tetragonal symmetry of the lattice, and hence the degenerate OP components of the unstrained crystal now have different condensation energies (and temperatures). Within weak coupling, a crystal under shear strain should therefore show two specific heat jumps[25], and, for a chiral OP, time-reversal symmetry breaking (TRSB) should set in at a different temperature than Meissner effect. Recent μ SR experiments[23] have indeed reported the latter effect. We show that the shear modulus jump can be related to $\Delta C/T$ (at zero strain) through the strain derivatives of these two transition temperatures, T_c and T_{TRSB} ,

$$\Delta c_s = -\frac{\Delta C}{T} \left| \frac{dT_1}{d\epsilon_s} \right| \left| \frac{dT_2}{d\epsilon_s} \right|, \quad (28)$$

where s is either B_{1g} or B_{2g} , $T_1 = T_c$, and $T_2 = T_{TRSB}$.

We start from the free energy expressions \mathcal{F}_{op} and \mathcal{F}_c , and consider the case $b_2 > 0, b_3 < b_2$, which leads to a chiral OP. Further, we keep only the coupling to $\epsilon_{B_{1g}}$ to simplify the subsequent algebra. Then, with the phase between η_x and η_y set to $\pi/2$, \mathcal{F}_{op} and \mathcal{F}_c are

$$\begin{aligned} \mathcal{F}_{op} &= a_0(T - T_{c,0})(\eta_x^2 + \eta_y^2) + b_1(\eta_x^2 + \eta_y^2)^2 + (b_3 - b_2)\eta_x^2\eta_y^2 \\ \mathcal{F}_c &= g_4\epsilon_{B_{1g}}(\eta_x^2 - \eta_y^2), \end{aligned} \quad (29)$$

where $T_{c,0}$ is the unstrained T_c . Clearly, $\epsilon_{B_{1g}}$ breaks the $\eta_x \leftrightarrow \eta_y$ symmetry of the quadratic terms in free energy, thereby making the two components condense at different temperatures.

We assume $g_4\epsilon_{B_{1g}} > 0$, which favors η_y condensing before η_x . The higher transition temperature $T_1 = T_c$ is determined by when the coefficient of η_y^2 goes to zero (with $\eta_x = 0$), that is, $a_0(T_1 - T_{c,0}) - g_4\epsilon_{B_{1g}} = 0$. This gives

$$T_1 = T_{c,0} + \frac{g_4}{a_0}\epsilon_{B_{1g}}. \quad (30)$$

Then, the η_y that minimizes $(\mathcal{F}_{op} + \mathcal{F}_c)$ is

$$\eta_y^2 = \frac{a_0(T_{c,0} - T) + g_4\epsilon_{B_{1g}}}{2b_1} = \frac{a_0(T_1 - T)}{2b_1}. \quad (31)$$

Further, the specific heat jump at this transition, calculated by using the above η_y^2 , is

$$\left(\frac{\Delta C}{T}\right)_1 = \frac{a_0^2}{2b_1}. \quad (32)$$

Below T_1 , the system undergoes TRSB transition when η_x condenses. Naively, one might expect this to occur at $T_{c,0} - g_4\epsilon_{B_{1g}}/a_0$, found by setting the quadratic coefficient of η_x to zero. The condensation of η_y prevents this, however, through the $\eta_x^2\eta_y^2$ terms in \mathcal{F}_{op} . If the coefficient of this term is zero ($2b_1 + b_3 - b_2 = 0$), then there is no competition between η_x and η_y , in which case the second transition does occur at $T_{TRSB} = T_{c,0} - g_4\epsilon_{B_{1g}}/a_0$.

For the more general case, when $2b_1 + b_3 - b_2 \neq 0$, $T_2 = T_{TRSB}$ is calculated by setting the coefficient of η_x^2 to zero in the total free energy, with η_y given by Equation 31. This gives

$$\begin{aligned} a_0(T_2 - T_{c,0}) + (2b_1 + b_3 - b_2)\eta_y^2 + g_4\epsilon_{B_{1g}} &= 0 \\ \implies T_2 = T_{c,0} - \frac{g_4}{a_0} \left(\frac{4b_1 - b_2 + b_3}{b_2 - b_3} \right) \epsilon_{B_{1g}} \end{aligned} \quad (33)$$

The specific heat jump at this transition can be calculated by subtracting the jump in first transition $(\Delta C/T)_1$ from the total jump $\Delta C/T$ in the unstrained case.

$$\left(\frac{\Delta C}{T}\right)_2 = \frac{2a_0^2}{4b_1 - b_2 + b_3} - \frac{a_0^2}{2b_1} = \frac{a_0^2}{2b_1} \frac{b_2 - b_3}{4b_1 - b_2 + b_3} \quad (34)$$

The ratio of the two specific heat jumps can then be related by

$$\left(\frac{\Delta C}{T}\right)_1 \bigg/ \left(\frac{\Delta C}{T}\right)_2 = \frac{4b_1 - b_2 + b_3}{b_2 - b_3} = \left| \frac{dT_2}{d\epsilon_{B_{1g}}} \right| \bigg/ \left| \frac{dT_1}{d\epsilon_{B_{1g}}} \right| \quad (35)$$

Below T_2 , the order parameter (η_x, η_y) can be calculated by minimizing $(\mathcal{F}_{op} + \mathcal{F}_c)$ with respect to both η_x and η_y . This gives

$$\begin{aligned} \eta_x^2 &= \frac{a_0(T_2 - T)}{4b_1 - b_2 + b_3} \\ \eta_y^2 &= \frac{a_0}{2b_1} \left((T_1 - T) - \frac{2b_1 - b_2 + b_3}{4b_1 - b_2 + b_3} (T_2 - T) \right) \end{aligned} \quad (36)$$

It is interesting to note that the condensation of η_x at T_2 decreases the rate at which η_y was growing below T_1 , demonstrating the competition between the two components (see Figure 8).

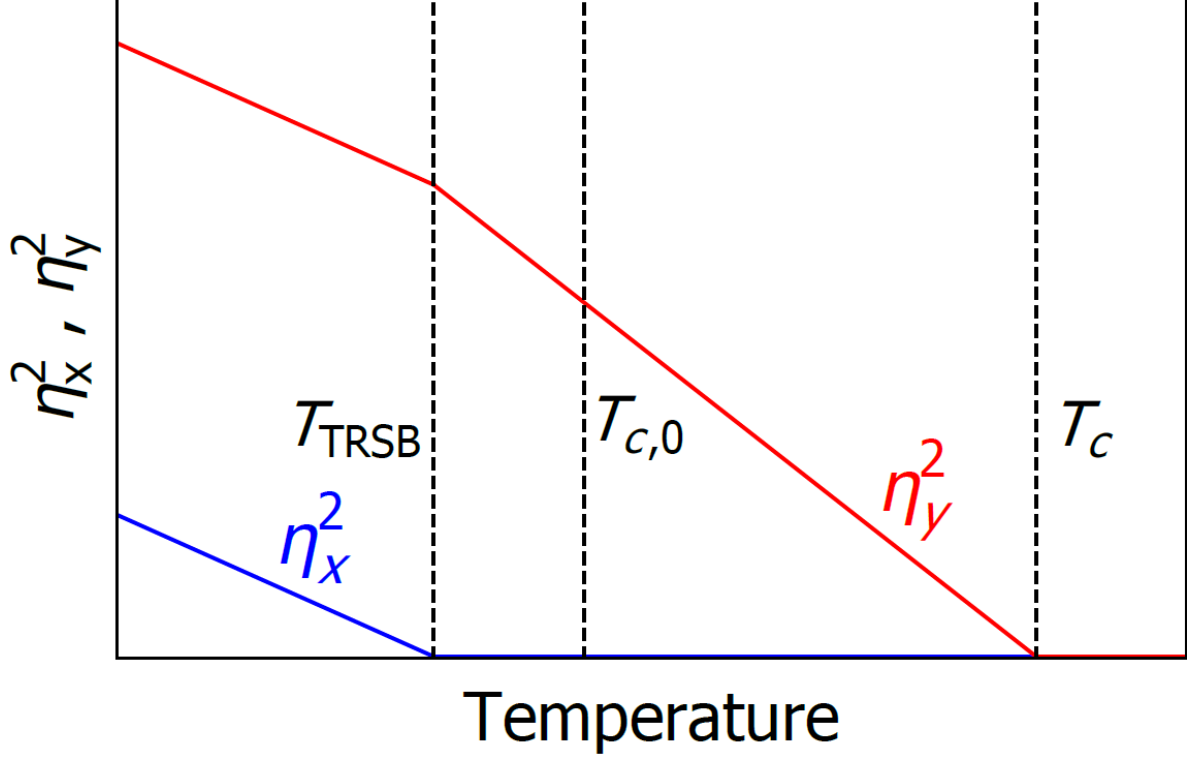


FIG. 8. **Strain-induced splitting of the transition temperature $T_{c,0}$.** Under B_{1g} shear strain, the two components η_y and η_x condense at different temperatures, T_c and T_{TRSB} , respectively. Above T_c , both the components are zero, and the sample is not superconducting. At T_c , the Meissner effect sets in, and finally, below T_{TRSB} , the system becomes a chiral superconductor. Note that the condensation of η_x decreases the rate at which η_y was growing below T_c . Qualitatively similar behavior is expected for B_{2g} shear strain, see text for details.

The jump in the B_{1g} shear modulus for chiral OP can now be expressed as,

$$\Delta C_{B_{1g}} = \frac{2g_4^2}{b_2 - b_3} = \frac{2a_0^2}{4b_1 - b_2 + b_3} \cdot \frac{g_4}{a_0} \cdot \frac{g_4}{a_0} \left(\frac{4b_1 - b_2 + b_3}{b_2 - b_3} \right) = -\frac{\Delta C}{T} \left| \frac{dT_1}{d\epsilon_{B_{1g}}} \right| \left| \frac{dT_2}{d\epsilon_{B_{1g}}} \right| \quad (37)$$

A similar derivation can be carried out for B_{2g} strain. This can be performed simply by re-defining the order parameter variables as $\tilde{\eta}_x = (\eta_x + \eta_y)/\sqrt{2}$ and $\tilde{\eta}_y = (\eta_x - \eta_y)/\sqrt{2}$ and carrying out the same calculation as the B_{1g} case.

The above derivation assumes that the spontaneous strains generated in the crystal below the first transition are small, such that the quartic coefficients in Landau theory are not strongly renormalized below T_1 . We also assume that the TRS-breaking transition under finite strain is a second order phase transition; whether this holds in Sr_2RuO_4 is a question for future studies.

Reconciling the c_{66} Discontinuity with Experiments Under Finite Strain

It follows from our measurement of a non-zero discontinuity in c_{66} that two transitions should occur under $\epsilon_{B_{2g}} = \epsilon_{xy}$ strain, each showing a specific heat jump, and T_c must split linearly with ϵ_{xy} strain (see Equation 30). However, past experiments[24, 25] have not observed either of these effects, and we comment on that here.

Experimental resolution of specific heat measurements under strain [25], and a lack of an observed discontinuity at a lower transition ($T_{\text{TRSB}} \equiv T_2$) gives a bound on the ratio of specific heat jumps at the purported transitions 1 and 2 as,

$$\left(\frac{\Delta C}{T}\right)_1 \bigg/ \left(\frac{\Delta C}{T}\right)_2 = \left| \frac{dT_2}{d\epsilon_{B_{2g}}} \right| \bigg/ \left| \frac{dT_1}{d\epsilon_{B_{2g}}} \right| \geq 20. \quad (38)$$

From the jumps in the B_{2g} modulus, $\Delta c_{66} \approx 10^6$ Pa, and in the specific heat, $\Delta C/T = 25$ mJ mol⁻¹ K⁻² ≈ 450 J m³ K⁻², we get

$$\left| \frac{dT_1}{d\epsilon_{B_{2g}}} \right| \bigg/ \left| \frac{dT_2}{d\epsilon_{B_{2g}}} \right| \approx 2000 \text{ K}^2. \quad (39)$$

From these two equations, we can estimate the shifts in the transition temperatures with strain as

$$\begin{aligned} \left| \frac{dT_1}{d\epsilon_{B_{2g}}} \right| &\leq 10 \text{ K} = 0.1 \text{ K}/\%_{\text{strain}} \\ \left| \frac{dT_2}{d\epsilon_{B_{2g}}} \right| &\geq 200 \text{ K} = 2 \text{ K}/\%_{\text{strain}} \end{aligned} \quad (40)$$

We can now compare these estimates to what has been experimentally observed. T_c as a function of ϵ_{xy} was reported in Hicks et al. [24], and the resolution on a possible cusp was 0.1 K/%; therefore the data of Hicks et al. [24] do not rule out a cusp of the magnitude predicted here. Furthermore, in recent μ SR experiments under applied B_{1g} strain[23], a modest suppression of T_{TRSB} is reported: ~ 0.2 K under a stress of -0.28 GPa, or a strain of $\sim -0.2\%$, for a slope of ~ 1 K/%. Although measurements under B_{2g} strain have not yet been reported, we note that this is comparable to the slope indicated above.